PHYSICAL REVIEW B **68**, 245416 (2003)

Reconstruction of charged surfaces: General trends and a case study of Pt(110) and Au(110)

Alexander Y. Lozovoi[1,2] and Ali Alavi[2]
[1]*Atomistic Simulation Group, School of Mathematics and Physics, The Queen's University of Belfast, Belfast BT7 1NN, Northern Ireland, United Kingdom*
[2]*University of Cambridge, Department of Chemistry, Lensfield Road, Cambridge CB2 1EW, United Kingdom*

(Received 27 July 2003; published 18 December 2003)

The stability of missing-row reconstructions of (110) surfaces with respect to surface charging has been investigated using *ab initio* theory, taking Pt and Au as representative systems. A thermodynamic formulation is derived to compare the relative stability of charged surfaces either in constant-potential or constant-charge mode. By generalizing Koopmans' theorem to charged metallic surfaces, we obtain an expression for the surface (excess) energy as a function of charge (or potential) in terms of the neutral surface energy, work function, and the position of the image plane. A surface is shown to reconstruct in constant-charge mode if and only if it reconstructs in constant-potential mode. We next address the question of whether a positive (negative) surface charge can lift (induce) the reconstruction, as suggested in the literature. This turns out not to be the case. Instead the following consistent picture arises: at small surface charges, the effect of the charge follows the difference of the work functions; i.e., positive charge favors a surface having a smaller work function and vice versa. Larger charges, either positive or negative, tend to stabilize the reconstructed surface or, more generally, the $1\times r$ reconstruction with larger r. The latter essentially results in that the 1×2 reconstruction in either Pt or Au is never lifted in our study, although the 1×3 surface in Au eventually becomes more stable.

DOI: 10.1103/PhysRevB.68.245416 PACS number(s): 68.35.Md, 68.35.Bs, 73.30.+y, 82.45.Fk

I. INTRODUCTION

In ultrahigh vacuum (UHV), the (110) surface of the late $5d$ metals Ir, Pt, and Au exhibits a 1×2 missing-row reconstruction, in which every other close-packed row in the $\langle110\rangle$ direction is missing. In some circumstances the 1×2 missing-row reconstruction can be lifted or, on the contrary, can develop a more severe 1×3 reconstruction (Fig. 1). The (110) surface of the isoelectronic $4d$ and $3d$ metals does not reconstruct, but the 1×2 missing-row reconstruction occurs on some of them (Ag, Cu, Pd, and Ni) upon a submonolayer adsorption of an alkali metal, such as Li, K, and Cs (see, e.g., Refs. 1 and 2 and references therein). Similar effects have been observed on the (100) surface, which under UHV conditions takes on a quasihexagonal ordering (called the 5×20 reconstruction), and also on the (111) surface (the $\sqrt{3}\times22$ reconstruction on gold, for example, which develops a distinctive "herringbone" pattern). A shared feature among all of these reconstructions is an increase in the density of atoms at the boundary between metal and vacuum (or electrolyte, if in the electrochemical environment). The 1×2 and 1×3 reconstructions, for instance, can be viewed as a transformation of the flat (110) surface into microfacets of the (111) surface, which is close packed.

The fact that a reconstruction appears for a number of different systems suggests that there may be general physical reasons behind it, rather than being dependent on specific details of the electronic structure of individual metals. Hence, three (possibly related) questions arise: (1) why do the surfaces of the end-of-the-row transition metals tend to reconstruct, (2) why does this tendency increase with row number, and (3) is there any physical quantity which can drive the reconstruction back and forward?

Here, we do not attempt to provide a complete overview of the long-standing discussion of this subject. We shall simply summarize the current understanding of the phenomenon, referring the reader to original papers and recent reviews (such as Refs. 3 and 4) for details. The answer to the

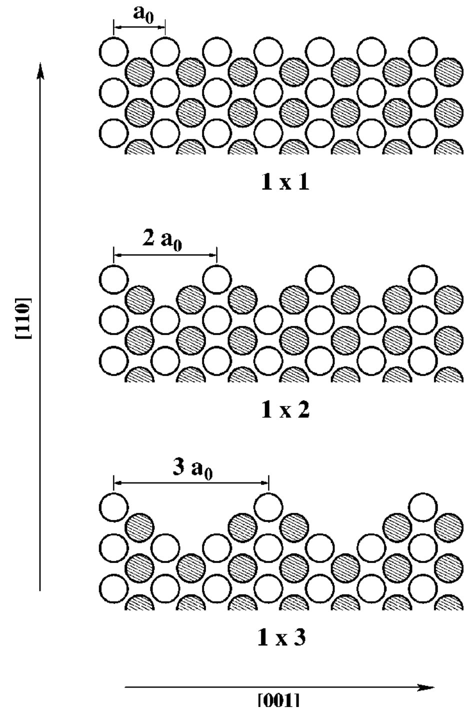

FIG. 1. Missing-row reconstruction at the (110) surface of fcc metals (side view). Shadowed and white atoms lie in planes displaced by $a_0/\sqrt{2}$ orthogonal to the plane of the picture, where a_0 is the lattice constant of the bulk crystal.

0163-1829/2003/68(24)/245416(18)/$20.00

first question seems to lie in the peculiar character of the interatomic interaction in metals with nearly filled d shells.[5] The driving force for the reconstruction is the decrease in kinetic energy of the delocalized surface electrons when they are provided with a larger effective surface area.[6] The increase of the reconstruction tendency in going down the periodic table [question (2)] has been attributed to a relativistic effect.[7,8] Other consequences of this effect are still being discovered.[9]

The third question is directly related to the subject of the current paper and therefore requires more comments. In addition to invoking the 1×2 reconstruction at the (110) surface of $3d$ and $4d$ metals (see above), the alkali-metal adsorption can further transform the (already reconstructed) 1×2 surface of $5d$ metals to 1×3.[10] On the other hand, the missing-row reconstruction in the $5d$ metals has been found to disappear upon adsorption of CO, NO, and Cl_2 molecules: $1\times2\rightarrow1\times1$ (see, e.g., references in Ref. 11). Hence it is plausible to suggest that surface charge alone could be responsible for invoking or lifting the reconstruction.[1,6,10,12]

In this mechanism, the adsorbed alkali atoms act as electron donors, oversaturating the surface with electrons, whereas molecules like CO, Cl_2, etc., can be regarded as electron acceptors. In other words, *the addition of electrons favors the more reconstructed surface*: $1\times1\rightarrow1\times2\rightarrow1\times3$ (hereafter we shall refer to the $1\times r$ reconstructed surface with larger r as the surface with a more extended reconstruction or, simply, as the more reconstructed surface).

On the other hand, it is equally possible that the specific interaction between adsorbed atoms and the metallic surface affects the reconstructed state of the surface, and there exist strong arguments for that.[2,13] These two effects are commonly referred to as the *long-range* (surface charge driven) and the *local* (adsorbate driven) mechanisms of the surface reconstruction, respectively.

Electrochemical experiments could provide an independent way to address the problem, because charged surfaces are a necessary accessory there and also because platinum and gold are commonly used as electrodes. A large body of available experimental data shows that the reversible transformation between 1×2 reconstructed and 1×1 unreconstructed Au(110) surfaces appears at a positive potential (i.e., when the surface is positively charged), the actual magnitude of which is electrolyte dependent.[3] In addition, the $1\times2\rightarrow1\times3$ transformation has been found to occur at some negative potential.[14] The 1×2 surface of Pt, however, is surprisingly stable.[3,15]

Regarding the above dilemma of whether a surface charge or adsorbate-substrate interaction invokes (or lifts) the surface reconstruction, electrochemical studies are still unable to give a definite answer, as the discrimination between the two effects is as difficult as in UHV experiments. However, this can be achieved in a straightforward way within the first-principles density functional approach. Although there exist a number of electronic structure calculations in which the reasons for the missing-row reconstruction have been thoroughly investigated, only in few of them has their energy been directly calculated as a function of external charge.

Fu and Ho[12] suggested that the (110) surface of silver should undergo a $1\times1\rightarrow1\times2$ missing-row reconstruction at a negative surface charge of $0.03e$ per surface site, where e is the electron charge. Bohnen and Kolb[16] considered the (100) surface of gold and found a $1\times2\rightarrow1\times1$ transition at a positive charge of $-0.4e/(\text{surface site})$. According to another (unpublished) calculation of the Au(110) surface by Bohnen mentioned in Ref. 4, a $1\times2\rightarrow1\times1$ transition is expected at a positive charge of $-0.09e/(\text{surface site})$ and a $1\times3\rightarrow1\times2$ transition occurs at about $-0.04e/(\text{surface site})$: the 1×3 neutral surface has been found to be marginally more stable in this study.

Based on the results of an electrochemical study of the Au(111) surface with adsorbed organic molecules, Wu *et al.*[17] argue that the effect of adsorbate and charge are of comparable magnitude; hence the driving force for surface reconstruction should contain a contribution from both.

Such a conclusion suggests that a careful consideration must operate rather with a *tendency* than with a definite result. Therefore, one of the purposes of our study was to clarifying, using *ab initio* density functional theory (DFT) calculations, whether positive (negative) charging of the (110) surface of Pt and Au indeed always *favors* a less (more) reconstructed surface. Our results do not support such a conjecture for either constant-charge or constant-potential modes: these two modes correspond to different experimental conditions and must be treated differently, Sec. II.

More generally, we believe that many similar questions could be clarified in a relatively simple way as charged metallic surfaces in vacuum appear to be a thermodynamic system obeying rather simple rules, thanks to Koopmans' theorem. It will be shown, in particular, that the behavior of surface energy of a charged system can be satisfactorily described if only properties of a neutral system are known. In Sec. III A we discuss the underlying thermodynamics within the previously developed model[18] in which the charged surface is represented by Guggenheim's surface layer plus an electric field stored outside in a *finite* region of vacuum. A generalization of Koopmans' theorem to charged surfaces within the above model constitutes Sec. III B. Section III C describes how to use the results of DFT supercell calculations as input for the model. The discussed corrections are further summarized specifically for the case of reconstruction energies in Sec. III D. Computational details are given in Sec. IV.

The rest of the paper concerns conclusions that can be drawn from the model and *ab initio* data. Using the example of (110) surfaces of platinum and gold, in Sec. V we discuss general features of the behavior of charged surfaces. Regarding the surface reconstruction, adding electrons should favor a surface with larger work function at small charges. For larger charges, a more extended reconstruction is favored at both positive and negative charge. The free-energy differences are qualitatively similar in constant-charge (Sec. V B 1) and constant-potential (Sec. V B 2) modes. In Sec. V B 3 we demonstrate that if surface energy curves intersect in one mode, they should cross in the other as well. This leads to a fascinating prediction of the possibility of the phase separation of charged surfaces forming coexisting domains with different reconstructions and different densities of the surface charge. In Sec. V C we briefly discuss the effect of field-induced atomic relaxation at a surface and conclude in Sec. VI.

II. CONSTANT-CHARGE OR CONSTANT-CHEMICAL POTENTIAL

When speaking about the relative stability of charged surfaces, one must distinguish between two possible situations. In the *constant-charge* mode, hereafter referred to as ''$N=\mathrm{const}$,'' the surface under investigation is maintained with a constant number of electrons, N_e. This means that, irrespective of the microscopic state of the surface, the total charge of the system remains unchanged. An example is the surface of a large sample of metal placed in a constant external electric field; to screen the field, charge accumulates at the surface, whose magnitude (per unit surface area) is determined by the magnitude of the applied field via Gauss's theorem.

The *constant-potential* mode (referred to as ''$\mu=\mathrm{const}$'') is the one in which the surface (the working electrode) is kept at a fixed potential relative to a reference system (the reference electrode). A physical realization is a parallel-plate capacitor connected to a battery, where one of the plates is the reference electrode and the other plate the system of interest. The battery fixes the potential difference between the two plates. In the language of density functional theory, this setup corresponds to the chemical potential of the electrons μ_e being fixed.

The difference between constant-charge and constant-potential modes has been noted by several investigators. Wu *et al.* in their study of the Au(111) surface reconstruction[17] recalculated the initial data to constant-charge mode. Symmetrically, to compare the reconstructed and unreconstructed Au(100) surfaces kept at the same potential, Bohnen and Kolb[16] converted the *ab initio* energy-charge curves into the energy-potential ones and found no crossover of the latter, whereas the former did cross. For the conversion, the authors employed experimental data in the capacity of a gold-electrolyte interface.

It is important to stress that the appropriate thermodynamic potential in the ''$\mu=\mathrm{const}$'' case is not the total (or free) energy, but rather its grand canonical equivalent. Indeed, if a system is allowed to fluctuate in N_e at fixed temperature and surface area, it requires a grand canonical description. A detailed discussion of the differences between the constant-charge and constant-potential modes and related computational aspects can be found in recent theoretical publications.[18–20]

III. THEORY

We shall be comparing the stability of $1\times r$ surfaces, where $r=1$, 2, or 3 denotes the extent of the surface reconstruction. The system to be considered is the surface region, large enough that its properties far from the surface match those of the bulk crystal to which it is attached, and similar on the vacuum side [Fig. 2(a)]. According to Guggenheim, this is referred to as the ''surface layer.''[21] In *ab initio* calculations, the surface layer of different surfaces will be represented with corresponding slabs [Fig. 2(b)].

The key feature of our thermodynamic model[18] is the way to deal with the divergence of the electrostatic energy of an infinite charged surface. This divergence is avoided by means of explicit inclusion of an oppositely charged electrode (the reference electrode) and hence of the electrostatic energy stored in the electric field in vacuum into the scheme [Fig. 2(a)]. A similar idea has been recently implemented within the jellium model framework by Ibach and Schmickler to calculate the step line tension on a metal electrode surface.[20] An alternative development within the embedded-atom method has been suggested by Haftel and Rosen[22] and applied to study the reconstruction of the Au(100) surface.[19]

A. Thermodynamics

For thermodynamic variables, we take pressure p, temperature T, and surface area A_0. The latter is understood as a projection of a ''real'' surface on the surface plane.[23] In the constant-charge mode one additionally has to specify the excess charge of the surface region q:

$$q=N_e-ZN_i\,, \tag{1}$$

where N_e and N_i are the number of electrons and ions, respectively, and Z is the ionic number (within the current paper, we only consider elemental crystals). In the constant-potential mode, the variable q is replaced with a surface electric potential $\mathcal{E}$, which is equal to the negative of the chemical potential μ_e of the electrons in the metal:[24]

$$\mathcal{E}=-\mu_e\,. \tag{2}$$

The above equation exemplifies a general problem in dealing with charged infinite systems—namely, the choice of the reference point to define the energy zero. For neutral surfaces or charged but finite systems,[25] the reference point can be safely specified at ''infinity''—i.e. an infinite distance away. Such a choice is no longer satisfactory if a surface is both infinite and charged: the chemical potential as well as the electrostatic energy at infinity diverges. A second important requirement for a proper definition of the energy zero is that the reference point must be consistent for the different surfaces; otherwise meaningful comparisons cannot be made.

A possible solution[18] is to set the electrostatic potential v_{es} to zero at some sufficiently large but finite distance Λ:

$$v_{es}(\mathbf{r})|_{z=\Lambda}=0, \tag{3}$$

where the z axis is normal to the surface. This can be achieved, for example, by placing an oppositely charged earthed electrode (the reference electrode) at Λ. The job of this electrode is twofold: (1) to terminate the electric field outside, and hence to make its energy finite, and (2) to define the energy zero independently of the surface considered. Since boundary condition (3) is adopted, the electron chemical potential μ_e becomes the energy required to remove an electron from inside the metal and place it at the plane $z=\Lambda$, where its electrostatic energy is zero by definition. Be-

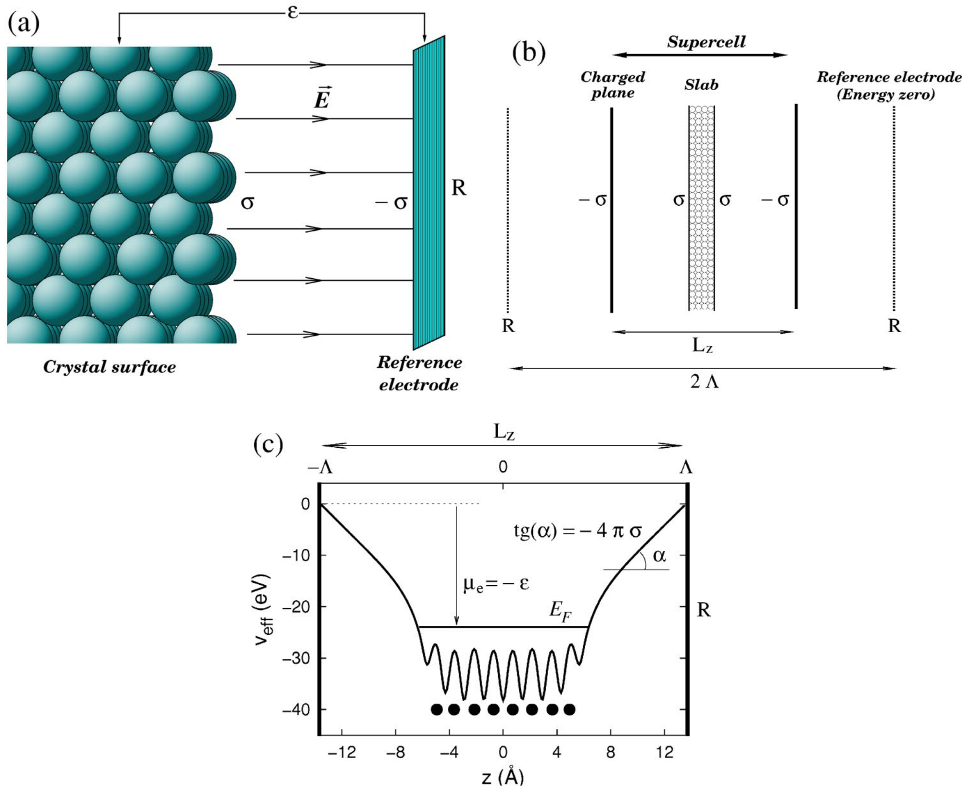

FIG. 2. (Color online) (a) A thermodynamic system considered in our study: metallic surface+reference electrode placed at some finite distance away. The energy stored in the electric field **E** in vacuum is a part of the total free energy of the system. (b) General setup used in the supercell calculations. The zero of electrostatic potential is defined by the position of the reference electrode *R*, characterized by the distance Λ measured from the center of the charged slab. Electroneutrality of the supercell is achieved by placing a plane of opposite charge on the cell boundary. The plane of countercharge need not coincide with the reference electrode *R* (although it does in the present study). After the self-consistent DFT calculation is done, the charged plane is removed, Eq. (30), and the effective potential v_{eff} is aligned such that $v_{es}(\pm\Lambda)=0$. (c) Planar-averaged effective potential of the gold 1×1 slab, processed as described above. The slab is charged positively, $\sigma=-0.1667e/(\text{surface site})$. Solid circles indicate the position of atomic layers. The reference electrode *R* is at the cell boundary: $\Lambda=L_z/2=13.61$ Å.

sides its mere convenience, the introduction of the reference electrode represents a real physical situation, in which a counterelectrode must be always present. In particular, the $\mathcal{E}$ variable acquires the meaning of the potential bias between the reference electrode and the surface of interest [Fig. 2(a)].

In the "$N=$const" mode, the most stable surface is the one which gives the lowest Gibbs free energy $G(p,T,A_0,q)$ of the corresponding surface layer. Finding the most stable surface is, in fact, minimization of a thermodynamic potential with respect to the extent of the surface reconstruction *r*, which plays here the role of a discrete internal variable. We then introduce the surface excess of the Gibbs free energy:

$$G^s(p,T,A_0,q)=G(p,T,A_0,q)-\mu_0(p,T)N_0, \qquad (4)$$

where $N_0=N_i$ is the number of atoms in the surface layer, and μ_0 is their chemical potential in the bulk of the metal. With the above definitions in mind and assuming that at each particular *r* the system is at local minimum and no external strain is applied to the sample, the surface excess Gibbs free energy G^s of our system can be shown to satisfy (see the Appendix)

$$G^s(p,T,A_0,q)=-\mathcal{E}q+\gamma A_0, \qquad (5)$$

$$dG^s=-S^s dT+V^s dp-\mathcal{E}dq+\gamma dA_0, \qquad (6)$$

where S^s and V^s are the surface excess entropy and volume, and γ denotes the surface energy (the reversible work of formation of unit area of new surface by cleavage).[26] In the thermodynamics of solid electrodes the latter is referred to as the superficial work.[23]

In the constant-potential mode, G^s has to be replaced by its grand-canonical equivalent J^s.[18–20] Application of the appropriate q-$\mathcal{E}$ Legendre transformation leads to

$$J^s(p,T,A_0,\mathcal{E})=G^s+\mathcal{E}q=\gamma A_0, \qquad (7)$$

$$dJ^s=-S^s dT+V^s dp+q d\mathcal{E}+\gamma dA_0; \qquad (8)$$

thus the surface energy γ times surface area A_0 is simultaneously the thermodynamic potential to minimize in the constant-potential mode.

If during the reconstruction A_0 does not change, comparing G^s or J^s is equivalent to comparing $g=G^s/A_0$ or $\gamma=J^s/A_0$, respectively.[27] From Eqs. (5) and (7),

$$\gamma(p,T,\mathcal{E})=g(p,T,\sigma)+\mathcal{E}\sigma, \qquad (9)$$

where $\sigma = q/A_0$ is the surface charge density. Due to Eq. (9), at $\sigma = 0$ (i.e., for a neutral system) both g and γ are equal and coincide with the standard definition of the surface energy for a neutral slab γ^0. Hereafter we shall be referring to g as the surface excess energy, while γ will be called just the surface energy.

From Eq. (6) and the definition of g and σ, it follows that

$$\left(\frac{\partial g}{\partial \sigma}\right)_{p,T,A_0} = -\mathcal{E}. \tag{10}$$

Similarly, from Eq. (8), the first derivative of the surface energy with respect to the potential bias is

$$\left(\frac{\partial \gamma}{\partial \mathcal{E}}\right)_{p,T,A_0} = \sigma. \tag{11}$$

Relation (11) is the Lippmann equation[28] (a particular case of the Gibbs adsorption isotherm for the case of charge excess), where we are using the sign convention that σ in Eq. (11) measures the surface charge in numbers of electrons: $\sigma < 0$ for positively charged surfaces, Eq. (1).

The second derivative of the surface energy defines the differential capacitance,[4]

$$(\partial^2 \gamma / \partial \mathcal{E}^2)_{p,T,A_0} = (\partial \sigma / \partial \mathcal{E})_{p,T,A_0} = -C, \tag{12}$$

and is related to the second derivative of the surface excess energy as

$$(\partial^2 \gamma / \partial \mathcal{E}^2)_{p,T,A_0} = -(\partial^2 g / \partial \sigma^2)^{-1}_{p,T,A_0}, \tag{13}$$

which is simply a property of the Legendre transformation (7).

B. Koopmans' theorem for a charged metal surface

Koopmans' theorem for metals states that the relation

$$\mu_e(\sigma = 0) = \varepsilon_F - v^0_{eff}(\infty) = -\phi \tag{14}$$

is exact.[30] Here ε_F is the position of the Fermi level and $v^0_{eff}(\infty)$ is the effective potential far from the surface—i.e., a vacuum zero. We shall be using the superscript zero to denote quantities which correspond to a neutral system (except the work function ϕ which is a property of a neutral surface).

For a charged surface, one can specify a reference state for an electron as being at some large but finite distance Λ from the surface (Sec. III A). Then it is possible to ask how much work is required to take an electron from inside the metal and put it at $z = \Lambda$. The same argument[30] of stationarity of the total energy with respect to an infinitesimally small perturbation of the electron density can be applied, and one arrives at

$$\mu_e(\sigma) = \varepsilon_F - v_{eff}(\sigma; \Lambda). \tag{15}$$

Ideally, calculating μ_e from either Eq. (15) or Eq. (10) should give identical results. This has been verified for both Pt(110) and Au(110) surfaces. The result for Pt is shown in Fig. 3.

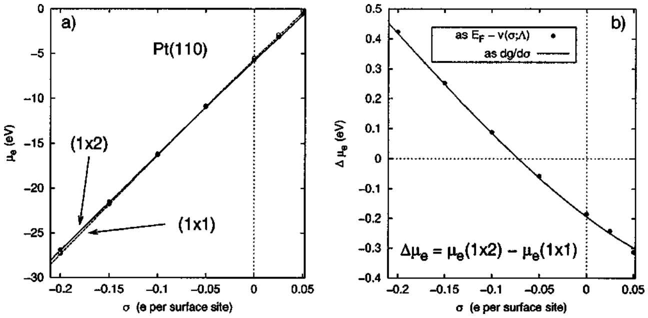

FIG. 3. Pt(110): (a) electron chemical potential μ_e as a function of charge obtained as a position of the Fermi level relative to the potential at the cell edges, Eq. (15) (circles), and as $\partial g/\partial\sigma$, Eq. (10) (lines). The solid line and solid circles correspond to the 1×2 reconstructed surface, the dashed line and open circles correspond to the 1×1 unreconstructed surface. The vertical dotted line marks the neutral slab: corresponding μ_e are the negative of the respective work functions (Table III). (b) Difference of the two curves shown in (a), $\Delta\mu_e = \mu_e(1\times 2) - \mu_e(1\times 1)$. Solid circles represent the difference of μ_e obtained from Eq. (15); the solid line gives the difference of the derivatives $\partial g/\partial\sigma$ of the respective surface excess energies interpolated separately. Note that slopes of $\mu_e(\sigma)$ curves are Λ dependent ($\Lambda = L_z/2 \simeq 12.54$ Å here), whereas $\Delta\mu_e(\sigma)$ does not depend on Λ. The plots demonstrate that both ways of calculating μ_e give similar results. The same level of agreement has been obtained for the gold surfaces (not shown).

An asymptotic form for an *xy*-averaged effective potential $v_{eff}(\sigma; z)$ of a surface carrying the charge density σ is given by a simple electrostatic expression[31–33]

$$v_{eff}(\sigma; z) = v^0_{eff}(z) - 4\pi\sigma[z - z_c(\sigma)], \tag{16}$$

where $z_c(\sigma)$ is the center of gravity of the excess surface charge $\delta\rho(\sigma; z) = \rho(\sigma; z) - \rho^0(z)$ of the semi-infinite crystal:

$$z_c(\sigma) = \frac{1}{\sigma}\int_{-\infty}^{+\infty} z\,\delta\rho(\sigma; z)\,dz. \tag{17}$$

Because of the form of Eq. (16), z_c is often referred to as the position of the image plane. Substituting Eq. (16) into (15) and identifying $v^0(\Lambda)$ with $v^0(\infty)$ for a neutral system, one arrives at

$$\mu_e(\sigma) = -\phi + 4\pi\sigma[\Lambda - z_c(\sigma)]. \tag{18}$$

Differentiating the above expression with respect to charge, one can find the differential capacitance of the metal–reference-electrode system as

$$C(\sigma) = \left[\frac{\partial \mu_e(\sigma)}{\partial \sigma}\right]^{-1} = \{4\pi[\Lambda - z_c(\sigma) - \sigma z_c'(\sigma)]\}^{-1}. \tag{19}$$

On the other hand, combining Eqs. (2), (10), and (18), we can integrate g to arrive at

$$g(\sigma) = \gamma^0 - \phi\sigma + 4\pi\int_0^{\sigma} t[\Lambda - z_c(t)]\,dt, \tag{20}$$

where by setting $\sigma=0$ we identify the integration constant γ^0 as the surface energy of a neutral system. Equations (18)–(20) can be considered as a *generalization of Koopmans' theorem to charged surfaces*.

Expression (20), in particular, proves to be extremely helpful in answering the main question of our study: namely, how the reconstruction energies depend on charge. Consider two different states of a surface: reconstructed *a* and unreconstructed *b*. In the difference of the respective energies the dependence on Λ disappears:

$$\Delta g(\sigma)\equiv g_a(\sigma;\Lambda)-g_b(\sigma;\Lambda)=\Delta\gamma^0-\Delta\phi\sigma -4\pi\int_0^{\sigma}t\Delta z_c(t)dt. \tag{21}$$

If we additionally neglect the dependence of Δz_c on charge $[\Delta z_c(\sigma)\simeq\Delta z_c^0]$, then we obtain $\Delta g(\sigma)$ as a quadratic function of σ:

$$\Delta g(\sigma)\simeq\Delta\gamma^0-\Delta\phi\sigma-2\pi\sigma^2\Delta z_c^0. \tag{22}$$

As we shall see below, the competition between the linear and quadratic terms largely determines the $\Delta g(\sigma)$ dependence for all the cases considered. Equation (22) tells one that the linear term favors a state with a larger work function for a negative charge ($\sigma>0$) and the state with a smaller work function for a positive charge ($\sigma<0$), whereas the quadratic term always favors a state having its extra charge farther away, irrespective of its sign. The latter is usually the case for a reconstructed surface as it becomes atomically rough (see Sec. V B 1). Equivalently, one can say that a reconstruction increases the capacitance of the metal +reference electrode system as

$$\Delta C^{-1}(\sigma)=-4\pi[\Delta z_c(\sigma)+\sigma\Delta z_c'(\sigma)]\simeq-4\pi\Delta z_c^0<0. \tag{23}$$

So far the above discussion referred to a constant-charge setup. Transition to the constant-potential mode is straightforward. From Eqs. (2), (9), and (18),

$$\gamma(\mathcal{E})=\gamma^0+4\pi\int_0^{\sigma(\mathcal{E})}t[\Lambda-z_c(t)]dt-\frac{(\mathcal{E}-\phi)^2}{4\pi[\Lambda-z_c(\sigma)]}, \tag{24}$$

where the $\sigma(\mathcal{E})$ dependence can be found from

$$\sigma[\Lambda-z_c(\sigma)]=\frac{\phi-\mathcal{E}}{4\pi}. \tag{25}$$

In particular, if $z_c(\sigma)\simeq z_c^0$, Eq. (24) simplifies to

$$\gamma(\mathcal{E})=\gamma^0-\frac{(\mathcal{E}-\phi)^2}{8\pi(\Lambda-z_c^0)}. \tag{26}$$

In this approximation,

$$\Delta\gamma(\mathcal{E})\simeq\Delta\gamma^0-\frac{1}{8\pi}\Delta\left(\frac{\phi^2}{\Lambda-z_c^0}\right)+\frac{1}{4\pi}\Delta\left(\frac{\phi}{\Lambda-z_c^0}\right)\mathcal{E} -\frac{\Delta z_c^0}{8\pi(\Lambda-z_{c_a}^0)(\Lambda-z_{c_b}^0)}\mathcal{E}^2; \tag{27}$$

i.e., at large potential the reconstructed state is again favored. It is important to note that the dependence of $\Delta\gamma$ on Λ does not disappear; in constant-μ mode, the distance between the metal and reference electrode is an essential parameter. Physically, the reason for this is obvious: differently charged surfaces generate different electric fields in vacuum whose energies do not cancel when subtracted.

C. DFT calculations

The *ab initio* contribution to the above scheme is to obtain the surface excess energy *g* as a function of the surface charge density $\sigma=q/A_0$ at a given external pressure *p* and temperature *T*. Within the present study, we consider the case of zero pressure $p=0$ and neglect all temperature effects originating from ions, although the temperature is treated explicitly for the electrons.[34]

1. General scheme

To find the surface excess energy *g*, one needs the Gibbs free energy of the surface layer *G* and the bulk Gibbs free energy per atom μ_0:

$$g(\sigma)=\frac{1}{A_0}[G(q)-\mu_0N_0]. \tag{28}$$

μ_0 can be easily obtained from a standard calculation of a neutral bulk material, whereas finding *G* is more tricky as it should be calculated such that the boundary condition, Eq. (3), in which Λ is measured from the center of the slab, is satisfied. In addition, if the self-consistent solution of the Kohn-Sham equations is sought within the supercell approach, each supercell should be neutral and include the plane of countercharge to neutralize a charged slab [Fig. 2(b)]. In practice, the distribution of the countercharge has finite width which results in an undesirable contribution to both the energy and effective potential of the cell.

We therefore consider the following steps to find $G(q)$.

(1) We temporarily assume that the reference electrode is at the cell boundary, $\Lambda=L_z/2$.

(2) At each particular value of *q* we find the self-consistent electron density $\rho(\mathbf{r})$ and corresponding effective potential $\tilde{v}_{eff}(\mathbf{r})$, the electrostatic part of which satisfies the boundary condition (3) with $\Lambda=L_z/2$, Fig. 2(c) (we use a tilde to mark the quantities which are the output of the electronic structure calculations for a neutralized cell).

(3) The correction due to the finite width of the countercharge is applied to the effective potential, energy, and the electron chemical potential, Sec. III C 2.

(4) The above quantities are recalculated to any arbitrary Λ (if needed), Sec. III C 3.

2. Correction due to the finite width of the Gaussian charge distribution

We assume that a charged slab is symmetric and centered around $z=0$, whereas the countercharge is distributed in thin sheets on the cell boundary with a Gaussian profile, width a:

$$\rho_G(\mathbf{r}) \equiv n_G(z) = -\frac{q}{Aa\sqrt{\pi}} \sum_{n\in Z} \exp\left[-\left(\frac{z-(2n+1)L_z/2}{a}\right)^2\right], \tag{29}$$

where A is the cell area parallel to the xy plane, L_z is the size of the cell along the z direction, and q is the charge of the slab. The width of the Gaussian is chosen to be small enough to avoid any charge overlap.

We align the electrostatic potential of the Gaussian planes $v_G(z)$ such that $v_G(\pm L_z/2)=0$:

$$v_G(z) = \frac{2\sqrt{\pi}aq}{A}[h(z)-h(L_z/2)],$$

where

$$h(z) = \exp\left[-\left(\frac{z-L_z/2}{a}\right)^2\right] + \exp\left[-\left(\frac{z+L_z/2}{a}\right)^2\right] + \sqrt{\pi}\left[\left(\frac{z+L_z/2}{a}\right)\mathrm{erf}\left(\frac{z+L_z/2}{a}\right) + \left(\frac{z-L_z/2}{a}\right)\mathrm{erf}\left(\frac{z-L_z/2}{a}\right)\right].$$

The effective potential due to the slab only, $v_{eff}(\mathbf{r})$, is then found by subtracting $v_G(z)$ from the "raw" effective potential $\tilde{v}_{eff}(\mathbf{r})$:

$$v_{eff}(\mathbf{r}) = \tilde{v}_{eff}(\mathbf{r}) - v_G(z). \tag{30}$$

If a is small enough (i.e., $L_z/a \gg 1$), $v_G(z)$ is flat everywhere in the cell apart from the small region near the cell edges. In particular, $v_G(z)$ is constant in the region occupied with the charged slab which ensures that after correction (30) the potential v_{eff} remains self-consistent.

The corresponding correction to the electrostatic energy of the slab E_{es} is

$$E_{es} = \tilde{E}_{es} + \sqrt{2\pi}\,\frac{aq^2}{A}, \tag{31}$$

where $\tilde{E}_{es}$ is the electrostatic energy given by supercell calculation.

In accordance with Eq. (30), the electron chemical potential μ_e calculated as a position of the Fermi level relative to the electrostatic potential at the cell boundary [i.e., by using Eq. (15)] can be obtained from the "supercell" one $\tilde{\mu}_e$ as

$$\mu_e = \tilde{\mu}_e + \frac{2\sqrt{\pi}aq}{A}. \tag{32}$$

TABLE I. Pt(110) neutral surface: convergence of the work function ϕ and surface energy γ^0 with respect to the slab width. N_{at} is the number of atoms per supercell: $N_{at}=16(20)$ corresponds to the 8(10) layer slab for the 1×1 surface and to the 9(11) layer slab for the 1×2 surface. Δ_N gives the difference between quantities corresponding to 16- and 20-atom slabs; Δ_{rec} is the difference between quantities corresponding to 1×2 and 1×1 slabs.

	ϕ (eV)			γ^0 (meV/Å^2)		
N_{at}	16	20	Δ_N	16	20	Δ_N
1×2	5.708	5.666	0.042	147.9	147.0	0.9
1×1	5.523	5.474	0.049	154.9	153.8	1.1
Δ_{rec}	0.185	0.192	-0.007	-7.0	-6.8	-0.2

3. Correction due to the reference plane position

This type of correction might be useful, for instance, if a particular position of the reference electrode has to be modeled, or, simply, if the surfaces to be compared were calculated using supercells of different size along z. So far we assumed that the reference electrode is placed at the distance $\Lambda=L_z/2$ measured from the center of the slab. This can be recalculated for any arbitrary Λ as

$$E_{es}(\Lambda) = E_{es}(L_z/2) + \frac{\pi q^2}{A}\left(\Lambda - \frac{L_z}{2}\right), \tag{33}$$

$$\mu_e(\Lambda) = \mu_e(L_z/2) + \frac{2\pi q}{A}\left(\Lambda - \frac{L_z}{2}\right), \tag{34}$$

where $E_{es}(L_z/2)$ and $\mu_e(L_z/2)$ are given by Eqs. (31) and (32), respectively (remember our sign convention: q gives the "electron charge" of the slab—i.e., $q<0$ if the slab is positively charged).

Formulas (33) and (34) are valid as long as the electronic charge density in the vacuum space between $z=\Lambda$ and $z=L_z/2$ is negligible. As we have already assumed that the electronic charge density of the slab at the cell boundaries $z=\pm L_z/2$ is vanishingly small, this condition is automatically satisfied for any $\Lambda>L_z/2$. If a smaller value of Λ is necessary, then some explicit modeling of the countercharge distribution might be recommended.

D. Reconstruction energy

In this section, we summarize for convenience the formulas of Sec. III C specifically for the case of the reconstruction energy calculations. Suppose that the *ab initio* simulation has been performed for two symmetric slabs S' and S'', representing two (differently) reconstructed surfaces, and refers to the situation in which the reference electrode is at distance Λ from the center of the slabs. The slabs contain N_0' and N_0'' atoms per periodic unit, which need not be equal. For simplicity, we assume that the both calculations were done using the same supercell dimensions $A\times L_z$; thus the surface area $A_0=2A$. As before, we assume that the electroneutrality of

TABLE II. Experimental and theoretical equilibrium bulk lattice constant a_0, work function ϕ, and surface energy γ^0 of Pt(110): unreconstructed (1×1) and reconstructed (1×2). In addition, the relaxation E_{rel} and reconstruction $\Delta\gamma^0$ energies are also listed: E_{rel} is the energy gain due to the relaxation of the surface atoms from their bulk truncated positions; the reconstruction energy is defined as $\Delta\gamma^0[(1\times m)\rightarrow(1\times n)]=\gamma^0(1\times n)-\gamma^0(1\times m)$, Eq. (35).

Method	LDA or GGA?	a_0 (Å)	ϕ (eV)		γ^0 (meV/Å^2)		E_{rel} (meV/Å^2)		$\Delta\gamma^0$ (meV/Å^2)	Ref.
			(1×1)	(1×2)	(1×1)	(1×2)	(1×1)	(1×2)	$(1\times1)\rightarrow(1\times2)$	
Experiment		3.92		5.84 [a]	(137.5) [b]				<0	
Sutton-Chen		3.92			67.6	66.6			-1.0	43
Potentials		3.92			68	67			-1.0	44
EAM		3.92			109					45
SEAM		3.92							-12.1	46
MEAM					123.7		9.6			47
TB		3.90			185					48
SKKR	LDA		6.10							49
LCAO	LDA	3.89	5.54		172					50
LMTO-FCD	GGA	4.019			176					51
Plane-wave	GGA	3.968		5.39	112		14	9.4		52
Pseudopot.	GGA	3.97							-8.7	53
	GGA	3.940			100	92			-8	54
	LDA	3.940	5.52	5.71	155	148	11	12	-7	Present study

[a] Reference 41.
[b] Polycryst., Ref. 42.

the cell is maintained by thin sheets of countercharge with a Gaussian half-width a placed between the periodic images of the slab.

On the output of the calculations, one has the Gibbs free energy of the system as a function of the slab charge, $\tilde{G}'(q)$ and $\tilde{G}''(q)$, and the electron chemical potentials, $\tilde{\mu}_e'(q)$ and $\tilde{\mu}_e''(q)$. These quantities are those taken directly from the supercell calculations; i.e., no electrostatic corrections have yet been applied. To decide which of the surfaces is more stable one has to find the sign of the difference of the relevant thermodynamic function of the both slabs. In constant-charge mode, this is the difference of the surface excess energies Δg at given charge q (or surface charge density $\sigma=q/2A$):

$$\Delta g(\sigma)\equiv g'(\sigma)-g''(\sigma)=\frac{1}{2A}[\Delta G(q)-\mu_0\Delta N_0], \qquad (35)$$

where $\Delta G(q)=\tilde{G}'(q)-\tilde{G}''(q)$ and $\Delta N_0=N_0'-N_0''$.

In constant-potential mode, one needs first to obtain the potential bias $\mathcal{E}$ between the slabs and the reference electrode as a function of the surface density of the excess charge σ,

$$\mathcal{E}(\sigma)=-\tilde{\mu}_e(q)-4\sigma[\sqrt{\pi}a-\pi(\Lambda-L_z/2)], \qquad (36)$$

and then invert the $\mathcal{E}(\sigma)$ dependence into the $\sigma(\mathcal{E})$ one. The more stable surface at given potential $\mathcal{E}$ can be then identified by looking at the sign of the surface energy difference $\Delta\gamma(\mathcal{E})$:

$$\Delta\gamma(\mathcal{E})\equiv\gamma'(\mathcal{E})-\gamma''(\mathcal{E})=\frac{1}{2A}[\Delta G(\mathcal{E})-\mu_0\Delta N_0]+\mathcal{E}\Delta\sigma(\mathcal{E})$$
$$+2\pi\left[\sqrt{\frac{2}{\pi}}a+(\Lambda-L_z/2)\right]\Delta\sigma^2(\mathcal{E}), \qquad (37)$$

where $\Delta G(\mathcal{E})=\tilde{G}'(q'(\mathcal{E}))-\tilde{G}''(q''(\mathcal{E}))$, $\Delta\sigma(\mathcal{E})=\sigma'(\mathcal{E})-\sigma''(\mathcal{E})$, and $\Delta\sigma^2(\mathcal{E})=\sigma'(\mathcal{E})^2-\sigma''(\mathcal{E})^2$.

Equation (35) shows that the relative stability of the surfaces kept at the same charge can be found using just the "raw" energies, $\tilde{G}(q)$, as it does not depend on Λ [cf. Eq. (21)]. Indeed, the energy of the electrostatic field stored outside the slab, which enters $\tilde{G}$ implicitly, cancels out if the surface charge density and the supercell size remain the same.[12] This is no longer the case for surfaces kept at the same potential, where some extra charge due to reconstruction (deconstruction) appears at the surface, the magnitude of which is Λ dependent, Eq. (36). Consequently, the electric field localized between the surface and the reference electrode becomes different, which contributes to the overall energy balance, Eq. (37).

IV. CALCULATION DETAILS

Free surfaces of Pt(110) and Au(110), unreconstructed (1×1) and reconstructed (1×2 and 1×3 for Au and 1×2 for Pt), were represented in our calculations by periodically repeated slabs constructed symmetrically to avoid any net dipole in the supercells. The charge of the slabs was balanced by planes of opposite charge with Gaussian distribution ($a=0.1$ Å) at the cell boundaries.

The lateral dimensions of the supercells were based on the

TABLE III. Experimental and theoretical equilibrium bulk lattice constant a_0, work function ϕ, and surface energy γ^0 of Au(110): unreconstructed (1×1) and reconstructed: (1×2) and (1×3). Definition of the listed quantities is the same as in Table II.

Method	LDA or GGA?	a_0 (Å)	ϕ (eV)			γ^0 (meV/Å^2)			E_{rel} (meV/Å^2)			$\Delta\gamma^0$ (meV/Å^2)		Ref.
			(1×1)	(1×2)	(1×3)	(1×1)	(1×2)	(1×3)	(1×1)	(1×2)	(1×3)	$(1\times1)\rightarrow(1\times2)$	$(1\times2)\rightarrow(1\times3)$	
Experiment		4.08		5.37 [a]			(83.20) [b]					<0	>0	
Sutton-Chen		4.08				40.3	39.7	39.8				-0.58	$+0.14$	43
Potentials		4.08				41	41					-0.62		44
EAM		4.08				61								45
		4.08				59.8	58.0					-1.87		55
SEAM		4.08				82.2						-6.2		22
MEAM		[4.08]				61.7			8.0					47
TB		4.06				115								48
SKKR	LDA		5.86											49
Mixed-basis	LDA	4.10				86.1	81.8		3	6		-4		6
Pseudopot.	LDA					83.0	78.0	77.1	4.4	6.7	7.3	-4.9	-0.9	56
	LDA					86.8								16
LMTO-GF	LDA		5.40			111								57
LMTO-FCD	GGA	4.198				78.0								51
Plane-wave	LDA	4.09	5.41	5.38										37
Pseudopot.	LDA	4.051	5.39	5.38	5.32	97	91	92	4	5	5	-5	$+0.3$	Present study

[a] Reference 41.

[b] Polycryst., Ref. 42.

equilibrium lattice constants taken from bulk calculations (Tables II and III). Neutral surfaces were relaxed with respect to the positions of atoms which were then kept unchanged (‘‘frozen’’) upon charging. The neglect of the field-induced relaxation is quite common in the calculation of charged surfaces[12,35] and is well justified for relatively small fields. We shall give a brief account of the effect of this additional atomic relaxation in Sec. V C. The results presented in Sec. V B are for the frozen surfaces, as the neglect of the field-induced relaxation does not affect our conclusions qualitatively (for small fields also quantitatively).

In choosing the amount of vacuum, we arranged the supercell boundaries sufficiently far to ensure negligible overlap of the tails of electron distribution with the charged planes. Negatively charged slabs required special attention as, if the surface charge exceeds a certain value, electrons begin to leave the slab and gather at the plane of opposite charge. This effect is well-known in *ab initio* calculations:[36] it appears when the Fermi level rises above the effective potential at the plane of countercharge. In our study, the occurrence of such electron leakage was controlled by both checking the electron density profile and the position of the Fermi level. Whenever any leakage was detected, the result of a corresponding calculation was considered unphysical and removed from a subsequent analysis.

A novel requirement which arises when the energies of charged surfaces have to be compared is that the supercells must be constructed in a consistent manner such that chosen slab widths and vacuum would not introduce any additional contribution to the total energy. Otherwise this contribution, being of comparable magnitude with typical energy differences, can lead to artifactual results. As usual, whenever such a problem appears one needs to consult the experiment which simulations aim to model. In the experiment, the electrodes are clamped: only surface atoms can rearrange themselves to form a suitable $1\times r$ reconstruction. This led us to the following setup: 8-layer slabs separated with 10 (11) interlayer spacings of vacuum represented the 1×1 surface of Pt (Au) (two central layers were kept fixed), while the 1×2 surface of Pt (Au) was modeled with 9-layer slabs (the first and ninth layers contained missing rows) having the layers positioned in between the respective layers of the 1×1 slab (three central layers were kept fixed). These slabs were separated with 9 (10) interlayer spacings of vacuum. The 1×3 gold surface corresponded to a 10-layer slab, having 8 central layers aligned with the layers of the 1×1 slab (2 central layers fixed); the amount of vacuum was 9 interlayer spacings.

To verify the effect of the width of the slabs, a test calculation for neutral Pt surfaces was undertaken in which we increased the number of atomic layers but kept the vacuum and other parameters constant. The results of the test (Table I) estimate the absolute convergence of the work function as 0.05 eV, close to the estimation of a finite-size error of 0.04 eV given by Fall *et al.*[37] The difference of the work functions of reconstructed and unreconstructed surfaces converges much better (0.007 eV). A similar picture arises for the surface energies: the absolute convergence is within 1 meV/Å^2, whereas the reconstruction energy changes by only 0.2 meV/Å^2. Although not exhaustive, these estimates are germane for our later discussion, which relies on the numerical significance of the work function and surface energy differences.

In the lateral dimension, both the 1×1 and 1×2 cells of Pt were simulated with a (1×2) unit cell. For gold such a strategy would be too expensive, as it requires a (1×6) unit cell for all surfaces. Instead, we used (1×1), (1×2), and (1×3) cells to represent respective surfaces, correspondingly changing the Monkhorst-Pack *k*-point sampling of the Brillouin zone—that is, using the $6\times12\times2$, $6\times6\times2$, and $6\times4\times2$ meshes, respectively. For Pt, the $6\times4\times2$ mesh was employed. Bulk chemical potentials were obtained using the same supercells as in surface calculations.

The remaining details are as follows: the calculations were performed within the local density approximation (LDA) using the plane-wave pseudopotential method as implemented in the CPMD code.[38] The ionic cores of Pt and Au were represented by the optimally smoothed pseudopotential[39] and the Troullier-Martins pseudopotential,[40] respectively, with a 40 Ry (Pt) and 50 Ry (Au) plane-wave cutoff energy.

V. RESULTS

A. Neutral surfaces

Tables II and III compare our results for the work functions and surface energies with experimental data and other calculations. Experimental work functions usually cover a considerable range, as they are sensitive to the cleaness of the surface. For both Pt and Au, we list the experimental values given in the CRC handbook,[41] although other data could be also mentioned. Fall *et al.*,[37] for example, cite lower experimental results for the work function of Au(110): namely, 5.12 and 5.20 eV. In turn, in *ab initio* calculations the work function fluctuates with the thickness of the slab.[58,59] Within the estimated finite-size error of 0.05 eV (see Sec. IV), the work functions obtained in the present study are in good agreement with those reported in Refs. 37, 50, and 57, higher than in Ref. 52 and significantly lower than in Ref. 49. Our results show that the $1\times1\rightarrow1\times2$ reconstruction increases the work function of platinum, but leaves the work function of gold almost unaffected. The latter is slightly reduced by the $1\times2\rightarrow1\times3$ reconstruction.

Work functions are generally larger for surfaces with a higher surface density of atoms. This is usually interpreted in terms of Smoluchowski smoothing[60]: electrons redistribute to a certain extent in between the surface atoms, thus lowering the surface dipole barrier. Applying this argument to the case of missing-row reconstruction is less straightforward. On the one hand, the overall density of the surface atoms does become lower with the reconstruction, which can result in a lowering of the work function; on the other hand, the reconstructed surface forms close-packed (111) facets, which should make the work function larger. Roughly speaking, one can consider the change of the work function as the result of the competition between these two effects: the work function first increases on (111) facets, but then is lowered due to the redistribution of the electrons to the regions between $[\bar{1}10]$ ridges.

Regarding the surface energies, we are not aware of any experimental data corresponding to the (110) surface either for Au or for Pt. In the tables, we include an estimation of these for polycrystalline material near the melting temperature, given by Tyson and Miller.[42] Extrapolating the surface energy of gold to zero temperature[42] increases the value listed in Table III up to $93.6\ \text{meV/Å}^2$ $(1\ \text{eV/Å}^2 = 16.021\,77\ \text{J/m}^2)$.

The calculated results listed in the tables show some scatter. Semiempirical methods tend to give lower values than those obtained from first principles. Comparing the latter, it seems important whether or not the generalized gradient approximation (GGA) is employed. According to Ref. 51, using the GGA usually decreases the surface energy: the effect is small for simple metals and most pronounced in the end of the *d* series. We however are especially optimistic about the agreement of the *differences* of the surface energies obtained in the present study and in other *ab initio* calculations.[6,37,53,54,56] Regarding the work function differences, the small number obtained for Au(110)-1×2 and Au(110)-1×1 surfaces in our study, -0.01 eV, compares rather well with the result of Ref. 37, -0.03 eV, and also agrees with the reported[61] small difference of the potentials of zero charge obtained in the electrochemical experiment using perchloric acid solution (known for its weak ion adsorption), ≈-0.02 V.

The parameters of structural relaxation of the considered surfaces are in reasonable agreement with those obtained in other *ab initio* calculations and experimental studies. We do not reproduce these here, but the data are available from the authors upon request.

B. Charged surfaces

1. Constant charge

The dependence of the surface excess energy g on charge σ, after all the necessary corrections having been applied, is shown in Fig. 4 for 1×1 and 1×2 surfaces of gold. As the 1×2 curve always lies below the 1×1 we deduce that the reconstruction is not lifted. Some general features can be noted about the curves. They cross the $\sigma=0$ line at respective surface energies of the neutral systems, γ^0, with slope $(-\phi)$, Eq. (20). At negative charges (i.e., on the $\sigma>0$ side) they approach a minimum, which corresponds to $\mu_e=-\mathcal{E}=0$, Eq. (10). At this point the Fermi level coincides with the reference zero of energy; i.e., this is a maximum negative charge beyond which the electrons become free (“field emission”). The curvature is everywhere positive as $\partial^2 g/\partial\sigma^2 = C^{-1}>0$, Eqs. (12) and (13), where C is the differential capacitance of the system comprising the charged surface and the reference electrode. Both the curvature [Eq. (19)] and the position of the minimum [Eq. (25) with $\mathcal{E}=0$] depend on how one chooses the distance between the electrodes (the Λ parameter). However, the difference between two curves—and in particular, whether there is a crossover—does not depend on Λ [Eq. (21) or (35)]. The reconstruction energies $\Delta g(\sigma)$ for all cases considered are shown in Figs. 5 and 6. As is expected from Fig. 4, there is no crossover for the $1\times2\rightarrow1\times1$ transition in gold [Fig. 6(a)]: a crossover occurs where Δg changes sign. The 1×2 surface in Pt is

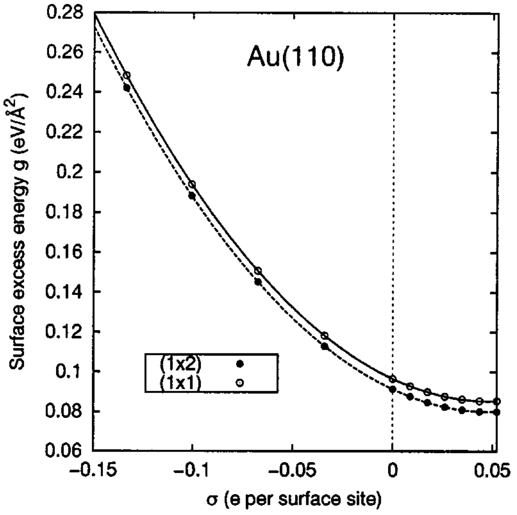

FIG. 4. Surface excess energy g of Au(110), Eq. (28) (constant-charge mode): 1×2 reconstructed (solid circles), and 1×1 unreconstructed (open circles). Solid and dashed lines represent a polynomial fit for the 1×1 and 1×2 surfaces, respectively. Respective curve for the 1×3 reconstructed surface is hardly distinguishable from that of the 1×2 surface on the scale of the plot. Vertical line denotes the neutral surface. The $g(\sigma)$ curves approach a minimum at $\mu_e=-\mathcal{E}=0$; their curvature is the reciprocal differential capacitance $1/C>0$, Eqs. (12) and (13). The plot shows that the missing-row reconstruction is never lifted.

also more stable than the 1×1 (Fig. 5). The only case of crossover we have encountered is for the 1×2 and 1×3 surfaces of gold [Fig. 6(b)].

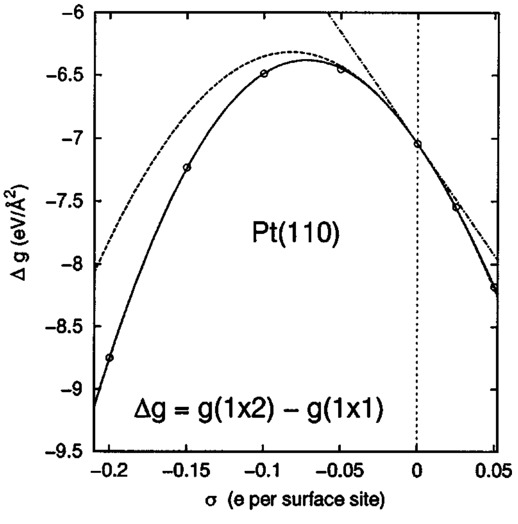

FIG. 5. Pt(110) in constant-charge mode: the difference of the surface excess energies of 1×2 and 1×1 surfaces, $\Delta g=g(1\times2)-g(1\times1)$ (solid line with open circles), and its approximation with linear (dash-dotted line) and quadratic (dashed line) terms, Eq. (22). Negative Δg means that the 1×2 surface is more stable. The vertical dotted line indicates the neutral surface. The slope of the tangent line gives the correct trend, whereas the second-order approximation (dashed line) satisfactory describes $\Delta g(\sigma)$ up to $|\sigma|\simeq0.05|e|$ per surface site. The plot indicates no lifting of the reconstruction, as $\Delta g(\sigma)$ never crosses zero.

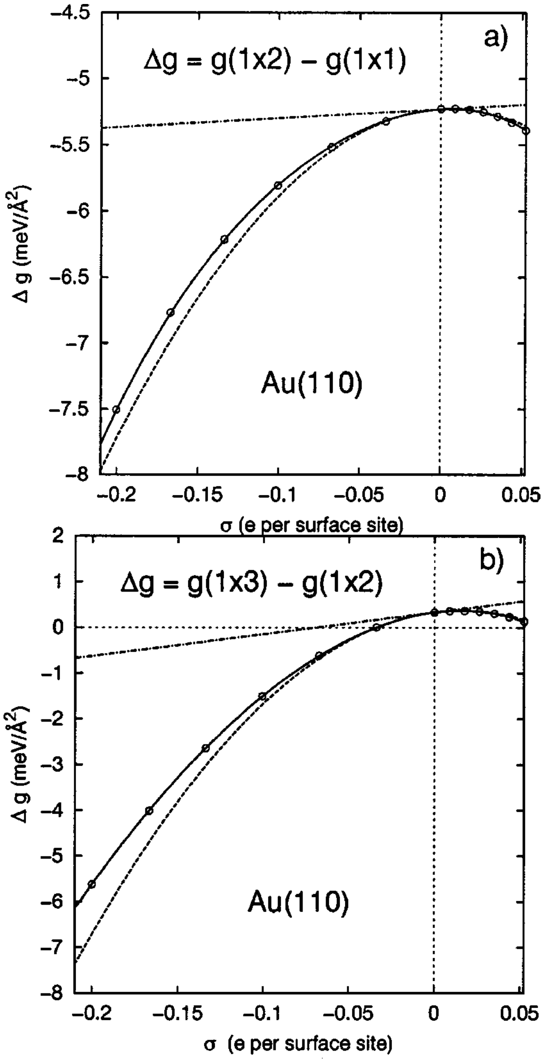

FIG. 6. Au(110): the difference of the surface excess energies of (a) 1×2 and 1×1 surfaces and (b) 1×3 and 1×2 surfaces (constant-charge mode). Notation is the same as in Fig. 5. The plots show that the 1×2 reconstruction is never lifted (a), but becomes less stable than the 1×3 reconstruction at a positive charge of $-0.034e$ per surface site (b). Note again that the quadratic approximation (dashed line) satisfactory reproduces the behavior of $\Delta g(\sigma)$ curves up to $|\sigma|\simeq0.05|e|$ per surface site.

It is convenient to analyze the general behavior of the $\Delta g(\sigma)$ curves in Figs. 5 and 6 in terms of Eq. (21). At $\sigma=0$, Δg approaches the difference of surface energies of the neutral systems, $\Delta\gamma^0$, with the slope $(-\Delta\phi)$. Hence, the difference of the work functions correctly describes the trend at small charges. Inclusion of a quadratic term (dashed lines in Figs. 5 and 6) appears to be a rather satisfactory approximation for $\Delta g(\sigma)$ in the whole range of charges and provides an almost perfect fit up to $|\sigma|\simeq0.05|e|$ per surface site [in our study $1|e|/(\text{surface site})=138.5$ μC/cm^2 for Au and 146.0 μC/cm^2 for Pt] which corresponds to electric fields slightly less than 1 V/Å . We thus continue our analysis using Eq. (22), which is Eq. (21) truncated at the second-order term. The coefficients in Eq. (22) are properties of the uncharged systems: the difference of surface energies $\Delta\gamma^0$, work functions $\Delta\phi$, and image-plane positions Δz_c^0. The latter is related to the difference of the inverse capacitances

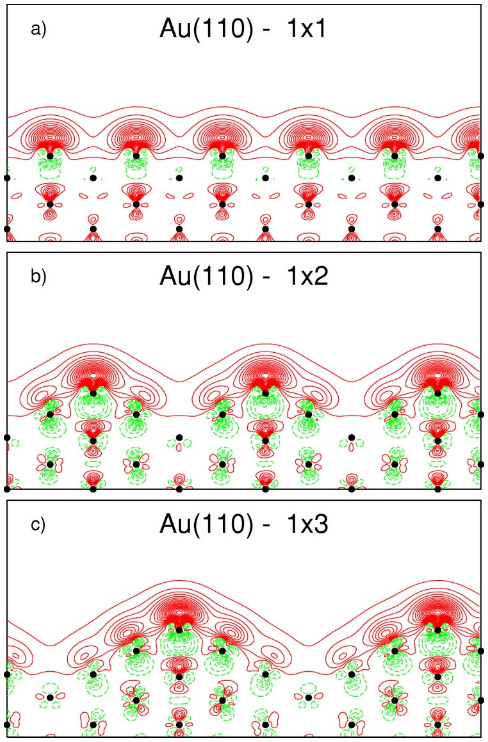

FIG. 7. (Color online) Location of excess charge at Au(110) surfaces: (a) 1×1, (b) 1×2, and (c) 1×3. Surfaces are charged positively with $\sigma=-0.052e$ per surface site. Contours start at $\pm5\times10^{-5}e/\text{a.u.}^3$ and are drawn with an increment of $10^{-4}e/\text{a.u.}^3$. Red solid and green dotted contours correspond to positive and negative charge, respectively. The sectioning plane is $(1\bar{1}2)$. Black dots show the positions of the ions. The buildup of the excess charge on top of the surface atoms contributes to σ^2 terms in the electrostatic energy and favors a surface with a more extended reconstruction. Same type of plots holds for negatively charged surfaces.

as $\Delta(1/C^0)=-4\pi\Delta z_c^0$. Therefore, if the surface energy, work function, and capacitance (or image-plane position) *for neutral systems* are known or can be reasonably estimated, the behavior of the charged ones can be predicted in much of the experimentally relevant range. A similar procedure is used in electrochemistry where the $\gamma(\mathcal{E})$ dependence is restored by means of the double integration of the $C(\mathcal{E})$ curve, taking the potential of zero charge as a substitute for the work function.[62]

Another feature seen in Figs. 5 and 6 is the negative curvature of all Δg curves, which means that large charges appear to favor a more reconstructed surface. In terms of Eq. (22), this is to say that a reconstruction should always move the image plane outwards or, equivalently, to increase the capacitance of the metal-surface–reference-electrode condenser. To understand the reasons behind this, we examine the redistribution of the excess charge density near the surface. This is shown in Fig. 7 for gold surfaces. The tendency for the excess charge to accumulate mainly on top of the surface atoms is clearly seen in the plots; the same trend has been noted in previous work.[12,63,64] Upon reconstruction, a surface becomes atomically rough, which means that some atoms move farther toward vacuum. The screening charge can redistribute itself to the top of these atoms and thus benefits in moving a certain distance along the electric field lines. The resulting energy gain is proportional to σ^2 and always favors reconstruction at sufficiently large charge. The same idea can be expressed in a simpler way: a reconstructed surface possesses an enhanced freedom in arranging its excess charge along the surface normal to minimize the surface energy.

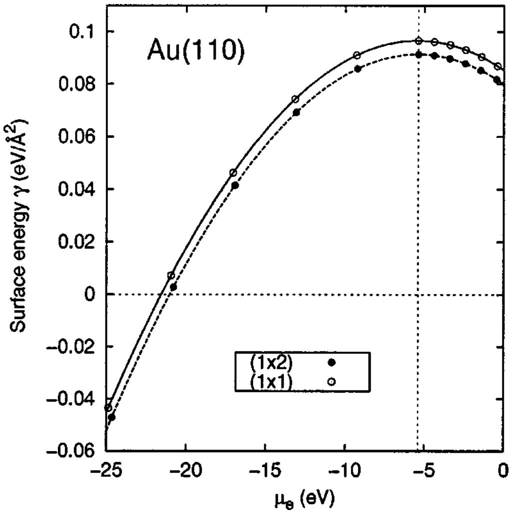

FIG. 8. Au(110): surface energy γ as a function of $\mu_e=-\mathcal{E}$ (constant-potential mode). Solid circles and dashed line correspond to the 1×2 reconstructed surface; open circles and solid line correspond to the 1×1 unreconstructed surface. Vertical dotted line denotes the neutral 1×2 surface. The curves are a maximum for respective neutral surfaces; their curvature is the negative of the differential capacitance C, Eqs. (12). Both the curvature of $\gamma(\mu_e)$ and the range of μ_e depend on parameter Λ (here $\Lambda=L_z/2\simeq13.61$ Å). Note that at large potential γ becomes negative, indicating system instability.

Being essentially electrostatic, the above argument should be equally applicable to other phenomena dealing with the outward displacement of part of the atoms on the interatomic distance scale. This can be compared to the results of Feibelman's recent calculations of adatom diffusion on Pt(100) in electric fields.[36] It was found that the farther an adatom lies from the surface, the faster its binding energy decreases with field.

To summarize, at small charges the effect of the charge follows the difference of the work functions, which can be of either sign. At larger charges, the more extended reconstruction is always favored. Overall, the effect of the charge is not sufficient to cause a reconstruction (by the exception of $1\times2\rightarrow1\times3$ transition in gold where the energy difference is indeed very small). A similar picture arises in constant-potential mode, which we consider next.

2. Constant potential

In Fig. 8 we plot the surface energy $\gamma(\mathcal{E})$ curves for the 1×1 and 1×2 surfaces of gold—i.e., analogous to those shown in Fig. 4 but in constant-potential mode. In accordance with Eq. (11), the curves are a maximum γ^0 at the

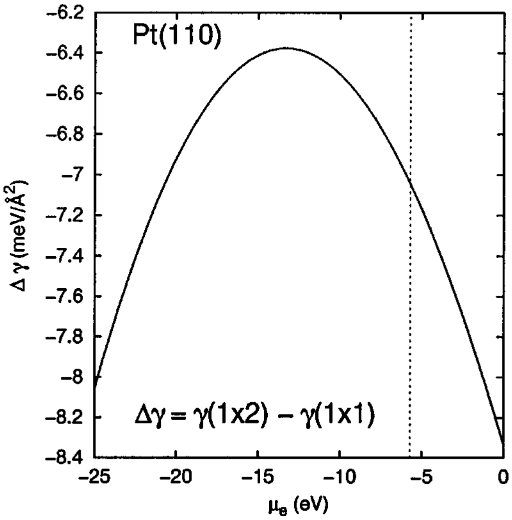

FIG. 9. Pt(110): the difference of the surface energies $\Delta\gamma$ of the 1×2 and 1×1 surfaces (constant-potential mode) for $\Lambda=L_z/2 \simeq 12.54$ Å. Contrary to the constant-charge case, $\Delta\gamma$ is Λ dependent: Equations (36) and (37) describe how to recalculate it from one Λ to another. The vertical dotted line indicates the position of the neutral 1×2 surface. Note the similarity in the behavior of the $\Delta\gamma$ and Δg curves (the latter is plotted in Fig. 5). In particular, the $\Delta\gamma$ plot does not show any lifting of the reconstruction in constant-potential mode either.

potential corresponding to neutral surfaces (the "potential of zero charge" in electrochemistry). The curvature of the parabolas is negative, in agreement with Eq. (12). The appropriate second-order approximation of the surface energy is given by Eq. (26).

An interesting new feature can be noticed in Fig. 8: at some stage γ becomes negative. This implies an instability of the system to create more surface. From a naive point of view such an effect seems natural: extra charge in metals always resides at the surface and hence produces electrostatic repulsion which should sooner or later overcome the cost of creating a new piece of surface. In practice, however, this type of instability will compete with another process leading to surface *destruction*: under the influence of a sufficiently large electric field charged ions start to escape from the surface. The latter phenomenon is well known (and extensively used) in field ion microscopy (FIM) experiments. In particular, this is exactly the way to prepare a (metastable) unreconstructed Pt(110) surface for low-temperature experiments.[65]

The behavior of $\Delta\gamma(\mathcal{E})$ curves (Figs. 9 and 10) is very similar to that of $\Delta g(\sigma)$ described previously (Figs. 5 and 6). The curvatures of Δg and $\Delta\gamma$ are of the same sign by virtue of Eq. (13): since C is positive, $\Delta C^{-1}>0$ if and only if $\Delta(-C)>0$. An important question is, however, whether the $g(\sigma)$ curves and the respective $\gamma(\mathcal{E})$ curves always intersect simultaneously. Indeed, this is precisely the case for all the systems considered here. But is this a general property? On the face of it, one might be tempted to say no, since in the constant-potential mode the reconstruction energies are Λ dependent, whereas in the constant-charge mode they are not. Perhaps, the similarity which we observe is simply due to the closeness of the work functions of reconstructed and unreconstructed surfaces? The correct answer is however, yes, but this is only half of the answer. We briefly consider this interesting issue in the next subsection.

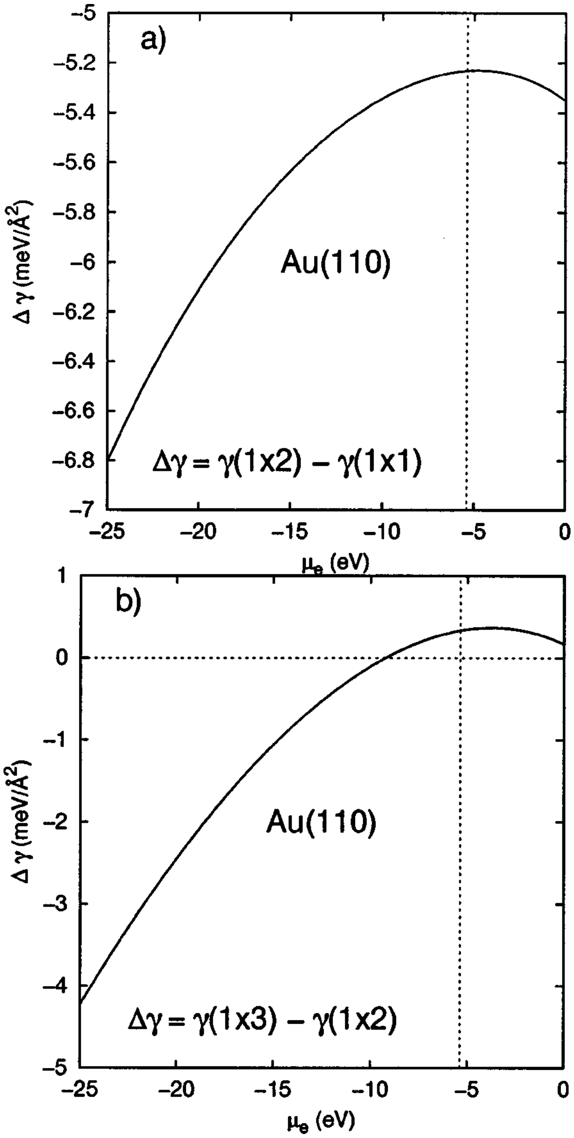

FIG. 10. Au(110): the difference of the surface energies $\Delta\gamma$ (a) of the 1×2 and 1×1 surfaces (i.e. those shown in Fig. 8) and (b) of the 1×3 and 1×2 surfaces (constant-potential mode). Notation is the same as in Fig. 9. Note again the similarity between this figure and Fig. 6, including presence or absence of the crossover.

3. Charge separation

The simplest way to attack the problem is to resort to the quadratic approximations of Δg and $\Delta\gamma$, Eqs. (22) and (27). If $g(\sigma)$ curves intersect in constant-charge mode, the quadratic (22) should have a non-negative discriminant. The same is true for $\Delta\gamma$, Eq. (27). After some tedious but straightforward algebra, one does arrives at the result that both discriminants are of the same sign, provided that $(\Lambda-z_c^0)$ is positive (as it must be). Other dependences on Λ in the "constant-potential" discriminant disappear, thus resolving the apparent paradox.

The above answer turns out not to be only restricted to quadratic approximations, but to have a rigorous thermodynamic reason. Suppose there is a crossing between two $g(\sigma)$ curves corresponding to two different surfaces in constant-charge mode, such as we found for the $1\times2\rightarrow1\times3$ transition in gold or $1\times1\rightarrow1\times2$ reconstruction in silver, as reported by Fu and Ho.[12] What happens to the system if the crossover charge σ_c is reached? The thermodynamically stable state in this case should be a *mixture* of two phases defined by a common tangent line drawn to the two $g(\sigma)$ curves. The slope of the tangent line gives the point at which $\gamma(\mathcal{E})$, the Legendre counterparts of $g(\sigma)$, intersect. This is akin to textbook examples considering the equilibrium of liquid-vapor mixture either at constant volume or constant pressure. Charge is an extensive variable and plays here the role of volume.

In the above reasoning we have neglected the energy of phase boundaries and possible interactions between domains of reconstructed surfaces. The former in fact defines the scale on which the phase separation takes place. Concerning the latter, it has been demonstrated by Vanderbilt[66] that the long-ranged domain-domain interaction always favors the phase separation due to its $1/r^3$ falloff.

To summarize, the behavior of surface energy differences $\Delta\gamma(\mathcal{E})$ in constant-potential mode is analogous to that of the surface excess energies $\Delta g(\sigma)$ in constant-charge mode. However, in contrast-charge mode, a phase coexistence of the two surfaces can occur over a range of σ, whereas in constant-potential mode, the surface is either fully reconstructed or unreconstructed depending of $\mathcal{E}$, except if one happens to lie precisely on the phase coexistence line, defined by the crossover condition $\Delta\gamma(\mathcal{E})=0$.

C. Field-induced surface relaxation

All the results mentioned so far have been obtained neglecting any additional atomic relaxation which can be brought upon by the surface charge. The effect of this approximation has been checked for the gold surfaces. As has been previously noted by Lam and Needs,[32] in large electrostatic fields, slabs dilate. We have obtained a similar result: up to surface charges of $(0.1–0.15)|e|/(\text{surface site})$ which correspond to fields of about 2 V/Å , the effect of the expansion is negligible. Thereafter it grows rapidly and its effect is to favor a more extended reconstruction. This is demonstrated in Fig. 11 in which we compare Δg obtained with and without the field-induced relaxation. Overall, the inclusion of relaxation makes the preference of a reconstructed surface at higher charges even more pronounced. The reasons for such behavior can be understood using the same electrostatic argument: atoms (essentially, ions) on reconstructed surfaces experience higher field due to the local enhancement effect and hence move farther. A related result was obtained by Neugebauer and Scheffler[67] who studied Na adatom on the Al(111) surface. They found that an electric field causes an outward displacement of the adatom which makes different adsorption sites (fcc hollow and on-top positions) nearly degenerate in energy at the electric field of 0.4 V/Å .

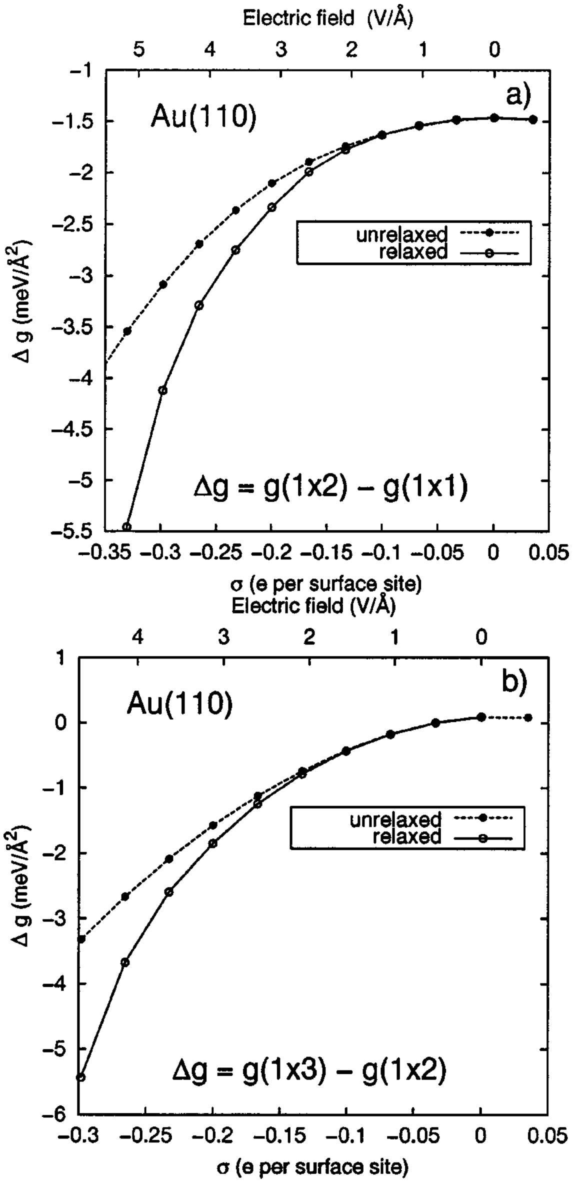

FIG. 11. Au(110): the reconstruction energy Δg as a function of the surface charge σ (a) for the $1\times1\rightarrow1\times2$ transition and (b) for the $1\times2\rightarrow1\times3$ transition. Dashed lines and solid circles correspond to surfaces initially relaxed at $\sigma=0$ and then kept "frozen" (same as in Fig. 6); solid lines and open circles represent the surfaces fully relaxed in an external field. The plots show that the effect of the field-induced atomic relaxation favors the surface with a more extended reconstruction.

If one continues to increase the charge on the surface, at a certain point the ions begin to escape, leading to field evaporation. This instability first arises for the 1×3 surface, then at higher field for the 1×2 surface, and finally for the unreconstructed 1×1 surface.

VI. CONCLUSIONS

In this paper we discuss general behavior and report calculation results of surface energy γ (constant-potential mode) and surface excess energy g (constant-charge mode) of reconstructed and unreconstructed (110) charged surfaces of platinum and gold.

(i) By the surface excess energy g we understand the energetic excess of a surface region (possibly carrying some charge) over the equivalent amount of (neutral) bulk material. This energy includes the energy stored in the electrostatic field outside the surface up to a certain reference plane, where we imagine having an ideal earthed oppositely charged plane, the reference electrode. The distance to the reference electrode is characterized by an additional (arbitrary) parameter Λ. Hence, g is the Gibbs free energy (per unit surface area) of a condenser. In constant-potential mode, the grand-canonical equivalent of g is needed: $\gamma = g + \mathcal{E}\sigma$. In our study, we call γ the surface energy; in the thermodynamics of charged electrodes, γ is referred to as the superficial work and indeed has the meaning of the surface energy (‘‘the reversible work of formation of new surface by cleavage’’[23]). There is a potential source of confusion regarding γ and g, as both reduce to the surface energy in neutral systems.

(ii) Combining the thermodynamic approach with Koopmans’ theorem (generalized to charge metal surfaces) allows one to express the surface (excess) energy of a charged system through the surface energy and work function of a neutral system and a position of the image plane. This allows one to access some general properties of $g(\sigma)$ and $\gamma(\mathcal{E})$ and their differences $\Delta g(\sigma)$ and $\Delta\gamma(\mathcal{E})$. In particular, the dependence of reconstruction energies on charge can be understood as a competition between the linear ‘‘work-function’’ and quadratic ‘‘image-plane’’ terms.

(iii) In all the cases considered, the behavior of the reconstruction energy is close to parabolic, especially in the region $|\sigma| \leq 0.05|e|$ per surface site. At sufficiently large charges the quadratic in σ term always favors $1\times r$ reconstruction with larger r. The reason for this appears to be of electrostatic origin: on the reconstructed surface, the screening charge can move farther along the lines of electric field, bringing upon a decrease in energy, quadratic in σ. The effect can be viewed as an increasing of the capacitance of the slab—reference-electrode system or as moving of the image plane outwards with reconstruction.

To first order in surface charge σ, adding electrons favors a surface with a larger work function. This conclusion does not support the statement discussed in the Introduction [adding electrons favors the (more) reconstructed surface]: they would have been equivalent if the reconstruction had always increased the work function. Such a correlation is not established at present; according to our results, Au represents a counterexample.

(iv) The behavior of the energy difference curves in constant-charge and constant-potential modes is qualitatively similar. In particular, if they cross zero in one mode, they should do so in the other mode as well. In our calculations, this was only observed for the $1\times2 \rightarrow 1\times3$ reconstruction in gold. For 1×2 surfaces of either Au or Pt, which are more stable than the 1×1 surfaces, the reconstruction can in principle be lifted only in the linear regime. However, the effect of the surface charge is not sufficient to overcome the energy difference and to lift the reconstruction.

(v) Finally, by analogy with the thermodynamics of bulk coexistence, we note here the remarkable possibility of the phase coexistence (in constant-charge mode) of two differently reconstructed surfaces carrying unequal density of surface charge, such that their integrated surface energies match. A possible candidate for this could be a $1\times2 \rightarrow 1\times3$ transition in gold although the respective energy gain is rather small. Fu and Ho’s results[12] on Ag(110) can be taken as a clue in looking for another system.

ACKNOWLEDGMENTS

The authors are indebted to Ruth Lynden-Bell for useful suggestions, inspirations, and a careful reading of the manuscript. Helpful discussions with Jorge Kohanoff, Cristián Sánchez, and Tchavdar Todorov are highly appreciated. We thank Michael Finnis for patiently clarifying difficult points we have encountered in the course of the work. The authors are obliged to Adrian Sutton for suggesting the coexistence of differently charged surfaces as a possible option. Michael Haftel is gratefully acknowledged for useful correspondence. We thank Peter Feibelman for a number of useful comments on the manuscript. This work was supported by the EPSRC via Grant Nos. M03931 and R89240. The Center for Supercomputing in Ireland is acknowledged for the provision of computer time on the IBM SP2 and the University of Cambridge for computer resources on the IBM SP3.

APPENDIX: THERMODYNAMIC POTENTIALS OF A CHARGED SURFACE IN CONSTANT-CHARGE AND CONSTANT-POTENTIAL MODES

In this appendix we present a detailed derivation of Eqs. (2) and (6)–(8) from Sec. III A.

1. Definitions and basic relations

We shall be referring to a system which consists of a surface layer, possibly charged, and an oppositely charged thin plane in vacuum at $z = \Lambda$ [Fig. 2(a)], where the z axis is normal to the surface. The energy of a neutral system does not depend on the zero of energy. It is convenient to define the energy zero by setting the electrostatic potential to zero at $z = \Lambda$, Eq. (3). As natural variables, we consider pressure p, temperature T, and surface area A_0. Any strain effects are neglected here, although can be incorporated along the lines of Ref. 29.

In the ‘‘$N = \mathrm{const}$’’ mode, we choose the number of ions, N_i, and electrons, N_e, as additional variables. The Gibbs free energy $G(p,T,N_i,N_e,A_0)$ is then an appropriate thermodynamic potential for our system. Thinking of the electrons and ions of the system as certain species,[24] we shall formally treat G in the same way as in multicomponent crystals,[68] namely,

$$G = \mu_e N_e + \mu_i N_i + \gamma A_0, \tag{A1}$$

where γ is the surface energy. Infinitesimal changes in the Gibbs free energy are given by

$$dG = -SdT + Vdp + \mu_i dN_i + \mu_e dN_e + \gamma dA_0. \tag{A2}$$

Equation (A2) can be taken as the definition of the layer quantities: the entropy S, volume V, chemical potentials μ_e and μ_i, and the surface energy γ. In particular, the chemical potential of electrons μ_e can be found as

$$\mu_e(p,T,A_0,N_i,N_e)=\left(\frac{\partial G}{\partial N_e}\right)_{p,T,A_0,N_i} \tag{A3}$$

and similarly for the ions. The physical meaning of μ_e is the minimal work required to remove an electron from inside the slab and put it at the reference plane at $z=\Lambda$, where its energy is zero by virtue of Eq. (3). For neutral surfaces μ_e becomes the negative of the work function ϕ provided that the plane $z=\Lambda$ is sufficiently far away in vacuum, which we assume is always the case. Hence, μ_e is a well-defined quantity. This conclusion equally applies to μ_i.

In the "$\mu=$const" mode the system is allowed to have variable number of electrons such as to bring the Fermi level to a desired position. Hence a grand-canonical description is suitable. The relevant thermodynamic potential J can be constructed from G by means of the Legendre transformation

$$\begin{aligned}J(p,T,\mu_i,\mu_e,A_0)&=G(p,T,N_i,N_e,A_0)-\mu_e N_e-\mu_i N_i\\&=\gamma A_0\end{aligned} \tag{A4}$$

or, in differential form,

$$dJ=-SdT+Vdp-N_i d\mu_i-N_e d\mu_e+\gamma dA_0, \tag{A5}$$

where we used Eq. (A1) in the second equality in Eq. (A4). The Gibbs-Duhem equation reads

$$A_0 d\gamma+SdT-Vdp+N_i d\mu_i+N_e d\mu_e=0. \tag{A6}$$

2. Charge-potential variables

The rather general consideration above can be simplified if one takes into account some additional properties specific for the system and species under consideration. First of all, up to the present point we have treated the variables N_e and N_i as independent. However, it will be recognized that the chemical potentials of electrons and ions are related:

$$Z\mu_e(p,T,N_i,N_e,A_0)+\mu_i(p,T,N_i,N_e,A_0)=\mu_0(p,T), \tag{A7}$$

where μ_0 is the chemical potential of the neutral atom. Equation (A7) expresses the fact that removing a nucleus of charge Z, together with Z electrons, amounts to removing a neutral atom from the bulk, and the work μ_0 required to do so is independent of the surface charge.

Relation (A7) represents an additional constraint on the thermodynamic variables. A simple way to take it into account in the constant-charge mode is to change the variables from (N_i,N_e) to (N_0,q):

$$N_i=N_0,\quad N_e=q+ZN_0, \tag{A8}$$

where q has the meaning of uncompensated (surface) charge and N_0 is the number of atoms in the surface layer.

In new variables, Eq. (A2) takes the form

$$dG=-SdT+Vdp+\mu_0 dN_0-\mathcal{E}dq+\gamma dA_0, \tag{A9}$$

where the chemical potential of the neutral atoms μ_0 and the potential bias $\mathcal{E}$ are related to μ_e and μ_i as

$$\mu_e=-\mathcal{E},\quad \mu_i=\mu_0+Z\mathcal{E}. \tag{A10}$$

The first equation in Eqs. (A10) is Eq. (2) of the main body of the paper (a derived result, not an assumption). The second equation gives the desired property (A7); in addition, N_0 and q are now fully independent variables.

A second useful property we wish to incorporate into the theory is the assumption that the surface layer is in equilibrium with the underlying bulk material.[69] According to the Gibbs phase rule, this should reduce the number of degrees of freedom (or the number of independent variables) by 1. Indeed, consider the Legendre transformation

$$G^s=G-\mu_0 N_0 \tag{A11}$$

followed by the application of the Gibbs-Duhem equation for the bulk crystal,

$$d\mu_0=-s_0 dT+v_0 dp,$$

where s_0 and v_0 are the bulk entropy and volume per atom. This eliminates μ_0 as an independent variable, leaving p, T, A_0, and q. In this way, we arrive at

$$G^s(p,T,A_0,q)=-\mathcal{E}q+\gamma A_0, \tag{A12}$$

$$dG^s=-S^s dT+V^s dp-\mathcal{E}dq+\gamma dA_0, \tag{A13}$$

where $S^s=S-N_0 s_0$ and similarly for V^s. The quantities marked with superscript s (calculated per the interface unit area) are *surface excesses*,[23,68] the reference component being the neutral atom. From Eqs. (A12) and (A13) one can easily obtain the Gibbs-Duhem equation in new variables:

$$A_0 d\gamma-q d\mathcal{E}+S^s dT-V^s dp=0. \tag{A14}$$

Instead of repeating the whole derivation in the constant-potential mode, one can take advantage of a convenient form of our previous expression for J, Eq. (A4), and use the Gibbs-Duhem equation (A14) to arrive at

$$J^s(p,T,A_0,\mathcal{E})=J(p,T,A_0,\mathcal{E})=\gamma A_0, \tag{A15}$$

$$dJ^s=-S^s dT+V^s dp+q d\mathcal{E}+\gamma dA_0, \tag{A16}$$

where the first equality in Eq. (A15) recognizes the fact that grand-canonical potentials are simultaneously the surface excess grand-canonical potentials.

Equations (A12) and (A13) are Eqs. (5) and (6) from the main body of the paper, whereas Eqs. (A15) and (A16) coincide with Eqs. (7) and (8), respectively.

[1] J.W.M. Frenken, R.L. Krans, J.F. van der Veen, E. Holub-Krappe, and K. Horn, Phys. Rev. Lett. **59**, 2307 (1987).

[2] R.J. Behm, D.K. Flynn, K.D. Jamison, G. Ertl, and P.A. Thiel, Phys. Rev. B **36**, 9267 (1987).

[3] D.M. Kolb, Prog. Surf. Sci. **51**, 109 (1996).

[4] W. Schmickler, Chem. Rev. (Washington, D.C.) **96**, 3177 (1996).

[5] V. Heine and L.D. Marks, Surf. Sci. **165**, 65 (1986).

[6] K.-M. Ho and K.P. Bohnen, Phys. Rev. Lett. **59**, 1833 (1987).

[7] N. Takeuchi, C.T. Chan, and K.M. Ho, Phys. Rev. Lett. **63**, 1273 (1989); Phys. Rev. B **43**, 14 363 (1991).

[8] V. Fiorentini, M. Methfessel, and M. Scheffler, Phys. Rev. Lett. **71**, 1051 (1993).

[9] H. Häkkinen, M. Moseler, and U. Landman, Phys. Rev. Lett. **89**, 033401 (2002).

[10] P. Häberle, P. Fenter, and T. Gustafsson, Phys. Rev. B **39**, 5810 (1989).

[11] H.P. Bonzel and S. Ferrer, Surf. Sci. **118**, L263 (1982).

[12] C.L. Fu and K.-M. Ho, Phys. Rev. Lett. **63**, 1617 (1989).

[13] K.W. Jacobsen and J.K. Nørskov, Phys. Rev. Lett. **60**, 2496 (1988).

[14] B.M. Ocko, G. Helgesen, B. Schardt, J. Wang, and A. Hamelin, Phys. Rev. Lett. **69**, 3350 (1992).

[15] C.A. Lucas, N.M. Marković, and P.N. Ross, Phys. Rev. Lett. **77**, 4922 (1996).

[16] K.P. Bohnen and D.M. Kolb, Surf. Sci. **407**, L629 (1998).

[17] S. Wu, J. Lipkowski, O.M. Magnussen, B.M. Ocko, and Th. Wandlowski, J. Electroanal. Chem. **446**, 67 (1998).

[18] A.Y. Lozovoi, A. Alavi, J. Kohanoff, and R.M. Lynden-Bell, J. Chem. Phys. **115**, 1661 (2001).

[19] M.I. Haftel and M. Rosen, Surf. Sci. **523**, 118 (2003).

[20] H. Ibach and W. Schmickler, Phys. Rev. Lett. **91**, 016106 (2003).

[21] E.A. Guggenheim, *Thermodynamics* (North-Holland, Amsterdam, 1959).

[22] M.I. Haftel and M. Rosen, Phys. Rev. B **64**, 195405 (2001).

[23] S. Trasatti and R. Parsons, J. Electroanal. Chem. **205**, 359 (1986).

[24] W. Schmickler and E. Leiva, J. Electroanal. Chem. **453**, 61 (1998).

[25] Y. Li, E. Blaisten-Barojas, and D.A. Papaconstantopoulos, Phys. Rev. B **57**, 15 519 (1998).

[26] For solid surfaces, Eq. (6) can also include the surface stress term as the surface area can be changed by means of elastic deformation. In our approach, the surface region is assumed to be attached to a semi-infinite bulk material maintained at equilibrium at given pressure and temperature. Hence, the surface area A_0 is linked to the equilibrium lattice constant of the bulk only, and no additional elastic deformation is permitted.

[27] The fact that g is the relevant quantity to compare different surfaces in the constant-charge mode was initially recognized by Parsons [R. Parsons, Proc. R. Soc. London, Ser. A **261**, 79 (1961)]. In electrochemical studies g is sometimes referred to as the Parsons function (Ref. 17).

[28] Generally, the Lippmann equation also contains the surface stress term (Ref. 29), for it is impossible experimentally to keep the surface strain constant while varying the surface charge (or potential bias), contrary to *ab initio* calculations. Despite neglecting any effect of elastic deformations (Ref. 26), our results are meaningful as in practice the stress term in the Lippmann equation is negligible [J. Lipkowski, W. Schmickler, D.M. Kolb, and R. Parsons, J. Electroanal. Chem. **452**, 193 (1998); R. Guidelli, *ibid.* **453**, 69 (1998)].

[29] P.R. Couchman and C.R. Davidson, J. Electroanal. Chem. **85**, 359 (1977).

[30] F.K. Schulte, J. Phys. C **7**, L370 (1974).

[31] N.D. Lang and W. Kohn, Phys. Rev. B **7**, 3451 (1973).

[32] S.C. Lam and R.J. Needs, J. Phys.: Condens. Matter **5**, 2101 (1993).

[33] M.W. Finnis, R. Kaschner, C. Kruse, J. Furthmüller, and M. Scheffler, J. Phys.: Condens. Matter **7**, 2001 (1995).

[34] A. Alavi, J. Kohanoff, M. Parrinello, and D. Frenkel, Phys. Rev. Lett. **73**, 2599 (1994).

[35] S. Heinze, X. Nie, S. Blügel, and M. Weinert, Chem. Phys. Lett. **315**, 167 (1999).

[36] P.J. Feibelman, Phys. Rev. B **64**, 125403 (2001).

[37] C.J. Fall, N. Binggeli, and A. Baldereschi, Phys. Rev. B **61**, 8489 (2000).

[38] CPMD, version 3.3, written by J. Hutter, A. Alavi, T. Deutsch, and the group of M. Parrinello at the MPI in Stuttgart and IBM research laboratory in Zürich.

[39] M.H. Lee, Ph.D. thesis, University of Cambridge, 1995.

[40] N. Troullier and J.L. Martins, Phys. Rev. B **43**, 1993 (1991).

[41] *CRC Handbook of Chemistry and Physics*, 78th ed., edited by D. R. Lide (CRC Press, Boca Raton, FL, 1998).

[42] W.R. Tyson and W.A. Miller, Surf. Sci. **62**, 267 (1977).

[43] I. Vilfan, F. Lancon, and E. Adam, Surf. Sci. **440**, 279 (1999).

[44] B.D. Todd and R.M. Lynden-Bell, Surf. Sci. **281**, 191 (1993); **328**, 170 (1995).

[45] S.M. Foiles, M.I. Baskes, and M.S. Daw, Phys. Rev. B **33**, 7983 (1986).

[46] M.I. Haftel, Phys. Rev. B **48**, 2611 (1993).

[47] J. Wan, Y.L. Fan, D.W. Gong, S.G. Shen, and X.Q. Fan, Modell. Simul. Mater. Sci. Eng. **7**, 189 (1999).

[48] M.J. Mehl and D.A. Papaconstantopoulos, Phys. Rev. B **54**, 4519 (1996).

[49] L. Szunyogh, B. Újfalussy, P. Weinberger, and J. Kollár, J. Phys.: Condens. Matter **6**, 3301 (1994).

[50] P.J. Feibelman, Phys. Rev. B **51**, 17 867 (1995).

[51] L. Vitos, A.V. Ruban, H.L. Skriver, and J. Kollár, Surf. Sci. **411**, 186 (1998).

[52] Q. Ge, W.A. Brown, R.K. Sharma, and D.A. King, J. Chem. Phys. **110**, 12 082 (1999).

[53] S.J. Jenkins, M.A. Petersen, and D.A. King, Surf. Sci. **494**, 159 (2001).

[54] O. Fitzpatrick, Ph.D. thesis, The Queen's University of Belfast, 2002.

[55] D. Wolf, Phys. Rev. Lett. **70**, 627 (1993).

[56] K.P. Bohnen and K.-M. Ho, Electrochim. Acta **40**, 129 (1995).

[57] H.L. Skriver and N.M. Rosengaard, Phys. Rev. B **46**, 7157 (1992).

[58] A. Kiejna, J. Peisert, and P. Scharoch, Surf. Sci. **432**, 54 (1999).

[59] C.J. Fall, N. Binggeli, and A. Baldereschi, J. Phys.: Condens. Matter **11**, 2689 (1999).

[60] R. Smoluchowski, Phys. Rev. **60**, 661 (1941).

[61] D.M. Kolb, in *Structure of Electrified Interfaces*, edited by J. Lipkowski and P.M. Ross (VCH, New York, 1993), p. 65.

[62] X. Gao, G.J. Edens, and M.J. Weaver, J. Electroanal. Chem. **376**, 21 (1994).

[63] J.E. Inglesfield, Surf. Sci. **188**, L701 (1989).

[64] S.C. Lam and R.J. Needs, Surf. Sci. **277**, 173 (1992).

[65] G.L. Kellogg, Surf. Sci. Rep. **21**, 1 (1994).

[66] D. Vanderbilt, Surf. Sci. **268**, L300 (1992).

[67] J. Neugebauer and M. Scheffler, Surf. Sci. **287**, 572 (1993).

[68] J.W. Cahn, in *Interfacial Segregation*, edited by W.C. Johnson and J.M. Blakely (American Society for Metals, Metals Park, OH, 1977).

[69] This assumption has been questioned by Lång and Heusler [G. Lång and K.E. Heusler, J. Electroanal. Chem. **377**, 1 (1994)] who noted that typical experimental times might be insufficient for a surface to reach equilibrium and suggested a way to take this into account [see also R. Parsons, Solid State Ionics **94**, 91 (1997)]. Here we consider only surfaces which are in equilibrium with the bulk material.